The implementation of Grover's algorithm in optically driven quantum dots

2006 J. Phys.: Condens. Matter 18 9975

(http://iopscience.iop.org/0953-8984/18/43/019)

INSTITUTE OF PHYSICS PUBLISHING JOURNAL OF PHYSICS: CONDENSED MATTER

J. Phys.: Condens. Matter **18** (2006) 9975–9986 doi:10.1088/0953-8984/18/43/019

The implementation of Grover's algorithm in optically driven quantum dots

W Yin[1,2], J Q Liang[2] and Q W Yan[1]

[1] Institute of Physics, State Key Laboratory of Magnetism, Beijing 100080, People's Republic of China
[2] Institute of Theoretical Physics, Shanxi University, Taiyuan 030006, People's Republic of China

E-mail: wyinsxu@sxu.edu.cn

Received 24 March 2006, in final form 8 September 2006
Published 13 October 2006
Online at stacks.iop.org/JPhysCM/18/9975

Abstract

In this paper, we study the implementation of Grover's algorithm using the system of three identical quantum dots (QDs) coupled by a multi-frequency optical field. Our result shows that increasing the electric field strength A speeds up the oscillations of the occupations of the excited states rather than increasing the occupation probabilities of those states. The larger the detuning of the field from resonance, the fewer the states which can be used as qubits. Compared with a multi-frequency external field, a single-frequency external field will generate much lower amplitudes of the excited states under the same coupling strength A and interdot Coulomb interaction V. However, when the three quantum dots are coupled with a single-frequency external field, these amplitudes increase on increasing the coupling strength A or decreasing the interdot Coulomb interaction V.

1. Introduction

In 1997 Grover discovered a quantum mechanical algorithm for the search problem, by which we can find an object in $\mathrm{O}(\sqrt{N})$ quantum steps instead of $\mathrm{O}(N)$ classical steps [1, 2]. Differing from Shor's algorithm of factorization [3], the superposition of single-particle quantum states is sufficient in Grover's algorithm. Leuenberger and Loss proposed that molecular magnets (for example, Mn_{12}) with non-equidistant energy levels could be used for implementing Grover's algorithm with the aid of advanced EPR techniques [4]. These systems can provide the quantum superposition of states with the same (at least the same magnitude of) amplitude by the use of a single pulse of a magnetic ac field containing an appropriate number of matched frequencies. An alternative version of Grover's algorithm is presented by them in [5] that exploits the properties of GaAs nuclei where electric quadrupolar interaction results in spin anisotropies and thus in non-equidistant energy levels. In addition, an exciting experimental work by Yusa *et al* [6] suggests that a self-contained NMR semiconductor device can control nuclear spins

in a nanometre-scale region, which can be applied to quantum search engines [4, 5, 7, 8] using Grover's algorithm based on the scheme presented by Leuenberger and Loss [4, 5].

In this paper, we give another solid-state realization of Grover's algorithm by using the optically generated electron–hole pairs (excitons) in semiconductor quantum dots. Recently, the combination of progress in ultrafast opto-electronics and in nanostructure fabrication has caused much studying of the coherent carrier control in semiconductor quantum dots [9, 10]. Theoretical studies [11–14] indicate that two different mechanisms can contribute to the coupling between the quantum dots: the resonant Fröster energy transfer and the direct Coulomb interaction between permanent excitonic dipole moments. When two quantum dots are separated by a distance less than the wavelength of light, the pulsed optical excitation of one QD leads to the reemission of a transient electric field which can be reabsorbed by the second QD; thus a resonant energy-transfer (Fröster) process transfers the excitation by which an exciton can hop between dots [15].

2. Theoretical model

We consider a system with three identical QDs. Ignoring any constant energy terms, the Hamiltonian describing the formation of single excitons within the individual QDs and their interdot hopping is the following [11]:

$$H(t) = H_I(t) + \frac{\varepsilon}{2}\sum_{n=1}^{3}(e_n^+ e_n - h_n h_n^+) + \frac{1}{2}V\sum_{n,n'}^{3}(e_n^+ h_{n'} e_{n'} h_n^+ + h_n e_{n'}^+ h_{n'}^+ e_{n'}) \tag{1}$$

where $H_I(t)$ is the optical field. $e_n^+(h_n^+)$ is the electron (hole) creation operator in the nth QD. ε is the QD band gap and V is the interdot Coulomb interaction, i.e. the Fröster process. Three dots are located at the vertices of an equilateral triangle, hence V is not relevant to the quantum dot 1, 2, or 3.

The study of dynamics of the system would be greatly simplified by introducing the quasispin operators

$$J_x = \tfrac{1}{2}\sum_{n=1}^{3}(e_n^+ h_n^+ + h_n e_n), \tag{2}$$

$$J_y = -\frac{\mathrm{i}}{2}\sum_{n=1}^{3}(e_n^+ h_n^+ - h_n e_n), \tag{3}$$

$$J_z = \tfrac{1}{2}\sum_{n=1}^{3}(e_n^+ e_n - h_n h_n^+), \tag{4}$$

which obey standard angular-momentum commutation relationships $[J_\alpha, J_\beta] = \mathrm{i}J_\gamma$, where (α, β, γ) represent a cyclic permutation of (x, y, z).

Applying the quasispin operators, the Hamiltonian can be rewritten as

$$H(t) = H_I(t) + \varepsilon J_z + V(J^2 - J_z^2). \tag{5}$$

The Hamiltonian includes a nonlinear term originating from Fröster process which results in non-equidistant energy levels (see figure 1). This is a necessary condition for the scheme of Leuenberger and Loss. The energy difference between the adjacent states is, therefore, shifted by $\pm 2V$ from ε. We define $|m\rangle \equiv |\frac{3}{2}, -\frac{3}{2}\rangle \equiv |0\rangle$, $|m\rangle \equiv |\frac{3}{2}, -\frac{1}{2}\rangle \equiv |1\rangle$, $|m\rangle \equiv |\frac{3}{2}, \frac{1}{2}\rangle \equiv |2\rangle$, $|m\rangle \equiv |\frac{3}{2}, \frac{3}{2}\rangle \equiv |3\rangle$, as the vacuum of the exciton, the single-exciton state, the biexciton state and the triexciton state, respectively.

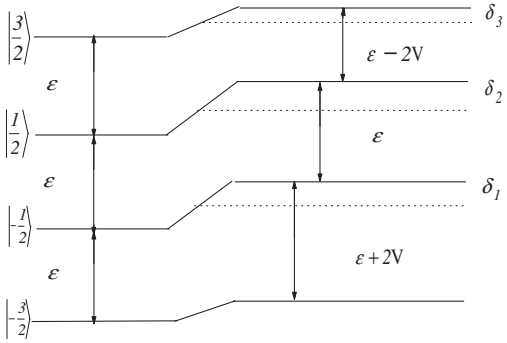

Figure 1. Schematic energy level diagram of the three quantum dots with (right) and without (left) the Fröster process.

3. Implementation of Grover's algorithm in three quantum dots coupled by a multi-frequency optical field

As the first step in deducing our scheme for implementing Grover's algorithm, we consider a multiphoton transition scheme for the coherent population of the J_z eigenstates $|m\rangle$ of a quasispin $J = \frac{3}{2}$. To induce the nth order transition from the vacuum state to the excited states $|m\rangle$, the field contains an appropriate number of frequencies $\{\omega_k\}$,

$$H_I(t) = A\mathrm{e}^{\mathrm{i}(\omega_1 t+\phi_1)}|-\tfrac{3}{2}\rangle\langle-\tfrac{1}{2}| + A\mathrm{e}^{\mathrm{i}(\omega_2 t+\phi_2)}|-\tfrac{1}{2}\rangle\langle\tfrac{1}{2}| + A\mathrm{e}^{\mathrm{i}(\omega_3 t+\phi_3)}|\tfrac{1}{2}\rangle\langle\tfrac{3}{2}| + \mathrm{H.c.}, \tag{6}$$

where $\omega_1 = \varepsilon + 2V - \delta_1, \omega_2 = \varepsilon + \delta_1 - \delta_2, \omega_3 = \varepsilon - 2V + \delta_2 - \delta_3$ and $\delta_1, \delta_2, \delta_3$ is the detuning of the field from resonance (see figure 1). A gives the electron–photon coupling and the incident electric field strength.

The time-evolution of the quantum state is governed by the Schödinger equation (where natural units are used throughout)

$$\mathrm{i}\frac{\mathrm{d}}{\mathrm{d}t}|\Psi(t)\rangle_s = H(t)|\Psi(t)\rangle_s. \tag{7}$$

Here we introduce the unitary transformation U:

$$|\Psi\rangle_s = U(t)|\Psi\rangle_U, \tag{8}$$

where we define the state in the rotating frame by $|\Psi\rangle_U = U^+|\Psi\rangle_s$. Thus, the left-hand side of equation (7) transforms into

$$\mathrm{i}\frac{\partial}{\partial t}|\Psi(t)\rangle_s = \mathrm{i}\left(U\frac{\partial|\Psi\rangle_U}{\partial t} + \frac{\partial U}{\partial t}|\Psi\rangle_U\right), \tag{9}$$

and the right-hand side of equation (7) transforms into

$$H_s|\Psi(t)\rangle_s = HU(t)|\Psi(t)\rangle_U. \tag{10}$$

Combining both sides of equations (9) and (10), we obtain

$$\mathrm{i}\frac{\partial|\Psi\rangle}{\partial t} = \left(U^{-1}HU - \mathrm{i}U^{-1}\frac{\partial U}{\partial t}\right)|\Psi\rangle_U = H_U|\Psi\rangle_U. \tag{11}$$

If we insert

$$\begin{aligned} U(t) = {} & \mathrm{e}^{\mathrm{i}[(\omega_1+\omega_2+\omega_3)t+(\phi_1+\phi_2+\phi_3)]/2}|-\tfrac{3}{2}\rangle\langle-\tfrac{3}{2}| + \mathrm{e}^{\mathrm{i}[(\omega_3+\omega_2-\omega_1)t+(\phi_3+\phi_2-\phi_1)]/2}|-\tfrac{1}{2}\rangle\langle-\tfrac{1}{2}| \\ & + \mathrm{e}^{\mathrm{i}[(\omega_3-\omega_2-\omega_1)t+(\phi_3-\phi_2-\phi_1)]/2}|\tfrac{1}{2}\rangle\langle\tfrac{1}{2}| + \mathrm{e}^{-\mathrm{i}[(\omega_1+\omega_2+\omega_3 t+(\phi_1+\phi_2+\phi_3)]/2}|\tfrac{3}{2}\rangle\langle\tfrac{3}{2}| \end{aligned} \tag{12}$$

we get the effective Hamiltonian in the rotating frame:

$$H_U = \begin{pmatrix} \frac{3}{2}V - \frac{\delta_3}{2} & \sqrt{3}A & 0 & 0 \\ \sqrt{3}A & \frac{3}{2}V + \delta_1 - \frac{\delta_3}{2} & 2A & 0 \\ 0 & 2A & \frac{3}{2}V + \delta_2 - \frac{\delta_3}{2} & \sqrt{3}A \\ 0 & 0 & \sqrt{3}A & \frac{3}{2}V + \frac{\delta_3}{2} \end{pmatrix}. \tag{13}$$

Here δ_1, δ_2 and δ_3 are the detuning parameters. We note the importance of the unitary transformation: the new Hamiltonian H_U is time independent. From a practical point of view, the parameters A and δ are adjustable in the experiment to give control over the system of QDs.

In resonance $\delta_1 = \delta_2 = \delta_3 = 0$, diagonalizing Hamiltonian (13) leads us to the following results:

$$\begin{aligned} |\varphi_{1,2}\rangle &= \eta_{1,2}\left[\left|-\frac{3}{2}\right\rangle + \frac{E_{1,2} - \frac{3}{2}V}{\sqrt{3}A}\left|-\frac{1}{2}\right\rangle + \frac{E_{1,2} - \frac{3}{2}V}{\sqrt{3}A}\left|\frac{1}{2}\right\rangle + \left|\frac{3}{2}\right\rangle\right], \qquad E_1 = \tfrac{3}{2}(2A + V), \\ &\quad E_2 = \tfrac{1}{2}(2A + 3V), \\ |\varphi_{3,4}\rangle &= \eta_{3,4}\left[\left|-\frac{3}{2}\right\rangle + \frac{E_{3,4} - \frac{3}{2}V}{\sqrt{3}A}\left|-\frac{1}{2}\right\rangle - \frac{E_{3,4} - \frac{3}{2}V}{\sqrt{3}A}\left|\frac{1}{2}\right\rangle - \left|\frac{3}{2}\right\rangle\right], \\ &\quad E_3 = -\tfrac{3}{2}(2A - V), \qquad E_4 = \tfrac{1}{2}(-2A + 3V), \end{aligned} \tag{14}$$

where the normalization constants

$$\eta_i = \frac{1}{\sqrt{2}}\left[1 + \left(\frac{E_i - \frac{3}{2}V}{\sqrt{3}A}\right)^2\right]^{-\frac{1}{2}} \tag{15}$$

and $i = 1, 2, 3, 4$.

In general, the total wavefunction can be expressed as

$$|\Psi(t)\rangle_U = \sum_k \sum_j C_k A_{kj} \mathrm{e}^{-\mathrm{i}E_k t}|m_j\rangle. \tag{16}$$

For Grover's algorithm, we must produce a superposition in which the amplitude of the N basic states is equal. We start from the initial state $|\Psi(0)\rangle = |-\frac{3}{2}\rangle$, i.e. we choose the zero-exciton state as the initial state. In this case, the wave function $|\Psi(t)\rangle_U$ is spanned by the following coefficients C_k and A_{kj}:

$$C_1 = \frac{1}{2\sqrt{2}}, \qquad C_2 = \frac{\sqrt{3/2}}{2}, \qquad C_3 = \frac{1}{2\sqrt{2}}, \qquad C_4 = \frac{\sqrt{3/2}}{2}, \tag{17}$$

and

$$A = \begin{pmatrix} \eta_1 & \eta_1 \frac{E_1 - \frac{3}{2}V}{\sqrt{3}A} & \eta_1 \frac{E_1 - \frac{3}{2}V}{\sqrt{3}A} & \eta_1 \\ \eta_2 & \eta_2 \frac{E_2 - \frac{3}{2}V}{\sqrt{3}A} & \eta_2 \frac{E_2 - \frac{3}{2}V}{\sqrt{3}A} & \eta_2 \\ \eta_3 & \eta_3 \frac{E_3 - \frac{3}{2}V}{\sqrt{3}A} & -\eta_3 \frac{E_3 - \frac{3}{2}V}{\sqrt{3}A} & -\eta_3 \\ \eta_4 & \eta_4 \frac{E_4 - \frac{3}{2}V}{\sqrt{3}A} & -\eta_4 \frac{E_4 - \frac{3}{2}V}{\sqrt{3}A} & -\eta_4 \end{pmatrix}. \tag{18}$$

The probability of finding the state $|m\rangle$ is given by

$$\rho(m) = |\langle m|\Psi(t)\rangle|^2 = \left|\sum_k C_k A_{km} \mathrm{e}^{-\mathrm{i}E_k t}\right|^2. \tag{19}$$

Figure 2 shows that the dynamic evolution of the system is characterized by the oscillation between $|-\frac{3}{2}\rangle$ and $|\frac{3}{2}\rangle$ with a much higher probability. Increasing the electric field strength A speeds up the oscillations of the occupations of the states. The larger A is, the larger the ν_{Rabi}

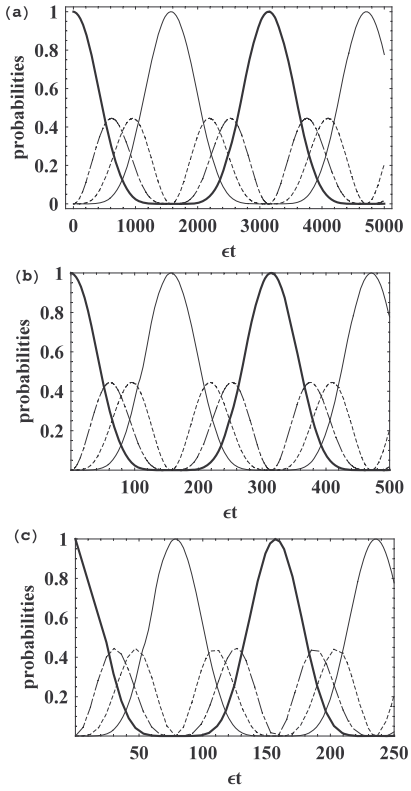

Figure 2. Time-evolution of the vacuum state $|-\frac{3}{2}\rangle$ (broad curve), the one-exciton state $|-\frac{1}{2}\rangle$ (dashed–dotted curve), the biexciton state $|\frac{1}{2}\rangle$ (dotted curve), and the triexciton state $|\frac{3}{2}\rangle$ (solid curve) in three coupled QDs, as a function of time. The energy is in units of the band gap ε and $\varepsilon = 1$. The initial state $|\Psi(0)\rangle = |-\frac{3}{2}\rangle$ in all figures except figure 7. (a) $A = 0.001\varepsilon$, $V = 0.1\varepsilon$, (b) $A = 0.01\varepsilon$, $V = 0.1\varepsilon$, (c) $A = 0.02\varepsilon$, $V = 0.1\varepsilon$.

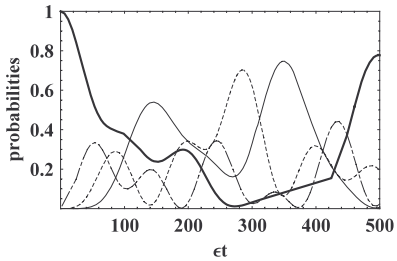

Figure 3. Time-evolution of the population of the vacuum state $|-\frac{3}{2}\rangle$ (broad curve), the one-exciton state $|-\frac{1}{2}\rangle$ (dashed–dotted curve), the biexciton state $|\frac{1}{2}\rangle$ (dotted curve), and the triexciton state $|\frac{3}{2}\rangle$ (solid curve) in three coupled QDs. The parameters are $\delta_1 = 2\delta_2 = 3\delta_3 = 0.03\varepsilon$, $A = 0.01\varepsilon$, and $V = 0.1\varepsilon$.

that can be achieved. However, it does not increase the amplitudes of the single-exciton state $|-\frac{1}{2}\rangle$ and the biexciton state $|\frac{1}{2}\rangle$ as we expect.

Then we consider the detuning of the field from resonance, $\delta_1 = 2\delta_2 = 3\delta_3 = 0.03\varepsilon$. Figure 3 shows that the resolution for identifying $|m\rangle$ is still sufficient and quite unexpectedly a

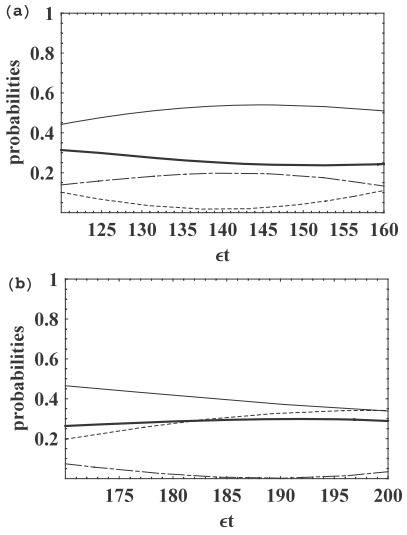

Figure 4. Grover's algorithm calculated by means of the analytical solution of equation (7). The probabilities of the vacuum state $|-\frac{3}{2}\rangle$ (broad curve), the one-exciton state $|-\frac{1}{2}\rangle$ (dashed–dotted curve), the biexciton state $|\frac{1}{2}\rangle$ (dotted curve), and the triexciton state $|\frac{3}{2}\rangle$ (solid curve) in three coupled QDs as a function of time: (a) $\varepsilon t = (120–160)$, (b) $\varepsilon t = (180–200)$. The parameters are $\delta_1 = 2\delta_2 = 3\delta_3 = 0.03\varepsilon$, $A = 0.01\varepsilon$, and $V = 0.1\varepsilon$.

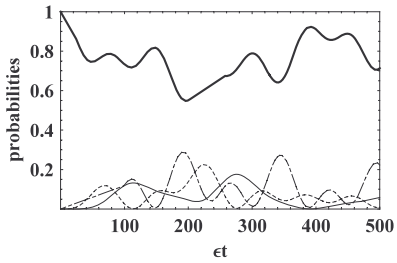

Figure 5. Time-evolution of the population of the vacuum state $|-\frac{3}{2}\rangle$ (broad curve), the one-exciton state $|-\frac{1}{2}\rangle$ (dashed–dotted curve), the biexciton state $|\frac{1}{2}\rangle$ (dotted curve), and the triexciton state $|\frac{3}{2}\rangle$ (solid curve) in three coupled QDs. The parameters are $\delta_1 = 2\delta_2 = 3\delta_3 = 0.06\varepsilon$, $A = 0.01\varepsilon$, and $V = 0.1\varepsilon$.

larger probability of biexciton state $|\frac{1}{2}\rangle$ can be achieved. Moreover, we can decode the number we want depending on a specific duration of the pulse (duration of the pulse $\varepsilon t = 120–160$ for 1011, $\varepsilon t = 180–200$ for 1101; see figures 4(a) and (b), respectively), where the probability $|a_m|^2 \geqslant 0.1$ is denoted 1 otherwise 0. When we enlarge the detuning of the field from $\delta_1 = 2\delta_2 = 3\delta_3 = 0.03\varepsilon$ to $\delta_1 = 2\delta_2 = 3\delta_3 = 0.06\varepsilon$, the probability of the vacuum state $|-\frac{3}{2}\rangle$ is much higher than those of the three excited states (see figure 5). This means we have indeed three states which can be used as qubits other than four states (or we can say the number we decode is always $\times\times\times 1$, where $\times$ is 0 or 1). Furthermore, the larger the detuning of the field from resonance, the fewer the states which can be used as qubits. When we enlarge the detuning up to $\delta_1 = 2\delta_2 = 3\delta_3 = 0.09\varepsilon$, according to our assumption, figure 6 shows the number we decode only can be 00×1. As a comparison to see the influence of the initial state on the implementation of Grover's algorithm, our calculation shows that the different initial

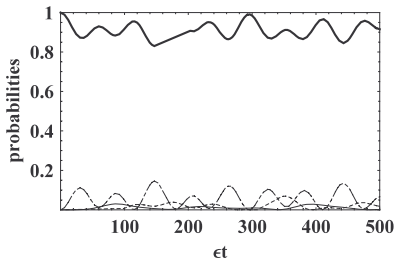

Figure 6. Time-evolution of the population of the vacuum state $|-\frac{3}{2}\rangle$ (broad curve), the one-exciton state $|-\frac{1}{2}\rangle$ (dashed–dotted curve), the biexciton state $|\frac{1}{2}\rangle$ (dotted curve), and the triexciton state $|\frac{3}{2}\rangle$ (solid curve) in three coupled QDs. The parameters are $\delta_1 = 2\delta_2 = 3\delta_3 = 0.09\varepsilon$, $A = 0.01\varepsilon$, and $V = 0.1\varepsilon$.

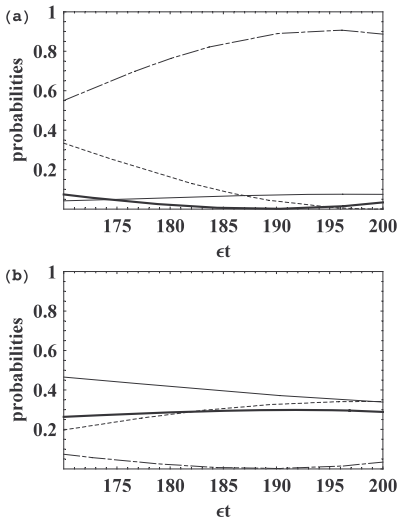

Figure 7. The implementation of Grover's algorithm with the different initial state. The probability of the one-exciton state $|-\frac{1}{2}\rangle$ (dashed–dotted curve), the biexciton state $|\frac{1}{2}\rangle$ (dotted curve), and the triexciton state $|\frac{3}{2}\rangle$ (solid curve) in three coupled QDs as the function of time $\varepsilon t = (180\ 200)$: (a) the initial state $|\Psi(0)\rangle = |-\frac{1}{2}\rangle$, (b) the initial state $|\Psi(0)\rangle = |-\frac{3}{2}\rangle$. The parameters are $\delta_1 = 2\delta_2 = 3\delta_3 = 0.03\varepsilon$, $A = 0.01\varepsilon$, and $V = 0.1\varepsilon$.

state will change the results of decoding. For the initial state $|\Psi(0)\rangle = |-\frac{1}{2}\rangle$, the duration of the pulse $\varepsilon t = (180\text{–}200)$ will decode the number 0010 instead of 1101 for initial state $|\Psi(0)\rangle = |-\frac{3}{2}\rangle$ (see figures 7(a) and (b), respectively).

The numerical calculations have been performed for all of the conditions mentioned above. As usual, we write

$$|\Psi(t)\rangle = \sum_m c_m(t) \mathrm{e}^{-\mathrm{i}\varepsilon_m t} |m\rangle, \tag{20}$$

where $\widehat{H_0}|m\rangle = \varepsilon_m|m\rangle$ and $\widehat{H_0} = \varepsilon J_z + V(J^2 - J_z^2)$. Thus the time-dependent Schrödinger equation is reduced to four first-order differential equations. Using the rescaled parameters $A' = A/\varepsilon, \delta_1' = \delta_1/\varepsilon, \delta_2' = \delta_2/\varepsilon, \delta_3' = \delta_3/\varepsilon$, and $\tau = \varepsilon t$, these four linear differential

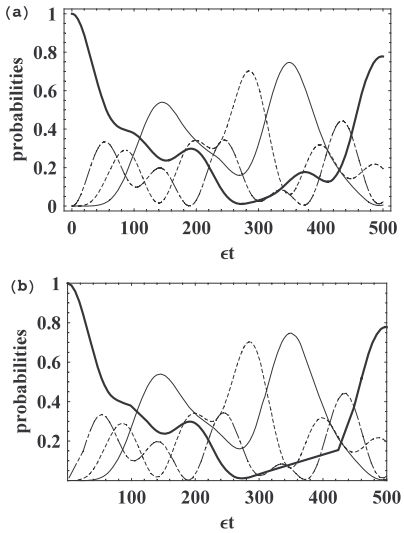

Figure 8. (a) Exact numerical and (b) analytical results of the time-evolution of the probability the vacuum state $|-\frac{3}{2}\rangle$ (broad curve), the one-exciton state $|-\frac{1}{2}\rangle$ (dashed–dotted curve), the biexciton state $|\frac{1}{2}\rangle$ (dotted curve), and the triexciton state $|\frac{3}{2}\rangle$ (solid curve) in three coupled QDs. The parameters are $\delta_1 = 2\delta_2 = 3\delta_3 = 0.03\varepsilon$, $A = 0.01\varepsilon$, and $V = 0.1\varepsilon$.

equations can be expressed in terms of reduced units as follows:

$$\begin{aligned}
\mathrm{i}\frac{\partial}{\partial\tau}a_{-\frac{3}{2}}(\tau) &= \sqrt{3}A' a_{-\frac{1}{2}}(\tau)\mathrm{e}^{-\mathrm{i}\delta_1'\tau},\\
\mathrm{i}\frac{\partial}{\partial\tau}a_{-\frac{1}{2}}(\tau) &= 2A' a_{\frac{1}{2}}(\tau)\mathrm{e}^{-\mathrm{i}(\delta_2'-\delta_1')\tau} + \sqrt{3}A' a_{-\frac{3}{2}}(\tau)\mathrm{e}^{\mathrm{i}\delta_1'\tau},\\
\mathrm{i}\frac{\partial}{\partial\tau}a_{\frac{1}{2}}(\tau) &= \sqrt{3}A' a_{\frac{3}{2}}(\tau)\mathrm{e}^{-\mathrm{i}(\delta_3'-\delta_2')\tau} + 2A' a_{-\frac{1}{2}}(\tau)\mathrm{e}^{-\mathrm{i}(\delta_1'-\delta_2')\tau},\\
\mathrm{i}\frac{\partial}{\partial\tau}a_{\frac{3}{2}}(\tau) &= \sqrt{3}A' a_{\frac{1}{2}}(\tau)\mathrm{e}^{-\mathrm{i}(\delta_2'-\delta_3')\tau}.
\end{aligned} \tag{21}$$

As an example, we give the numerical and the analytical solutions of equation (7) with the parameters $A = 0.01\varepsilon$, $V = 0.1\varepsilon$ and $\delta_1 = 2\delta_2 = 3\delta_3 = 0.03\varepsilon$. Figure 8 shows the excellent agreement for the probabilities of the four states.

4. Greenberger–Horne–Zeilinger state generation in three QDs

Next we describe the generation of the Greenberger–Horne–Zeilinger (GHZ) state [16]. To this end we assume that the states $|0\rangle$ and $|1\rangle$ represent the vacuum state and the excited state, respectively. The GHZ state is given by

$$|\Psi_{\mathrm{GHZ}}\rangle = \tfrac{1}{\sqrt{2}}\left(|0^{\otimes N}\rangle + |1^{\otimes N}\rangle\right), \tag{22}$$

which means a coherent superposition state of all QDs in mode $|0\rangle$ and all QDs in mode $|1\rangle$. This state is also known as the Schrödinger cat state, in honour of Schrödinger's quantum superposition of states-cat states. We can rewrite the GHZ state in the quasispin representation such that

$$|\Psi_{\mathrm{GHZ}}\rangle = \tfrac{1}{\sqrt{2}}\left(|-\tfrac{3}{2}\rangle + |\tfrac{3}{2}\rangle\right). \tag{23}$$

The probability to achieve the GHZ state $|\Psi_{\mathrm{GHZ}}\rangle$ at time t for our general solution of

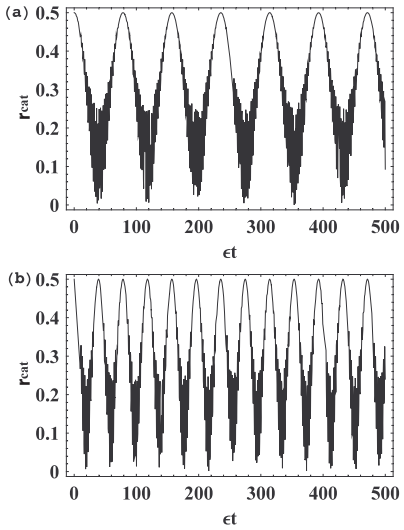

Figure 9. Generation of the GHZ state with different coupling strengths: (a) $A = 0.01\varepsilon$, (b) $A = 0.02\varepsilon$. The parameters are $\delta_1 = \delta_2 = \delta_3 = 0$ and $V = 0.1\varepsilon$.

equation (7) is seen to be

$$|\langle\Psi_{\mathrm{GHZ}}|\Psi(t)\rangle|^2 = \tfrac{1}{2}\left|\sum_k C_k(A_{k1} + A_{k4})\mathrm{e}^{-\mathrm{i}E_k t}\right|^2. \tag{24}$$

Figure 9 shows the probability to find the GHZ state in the QDs with various coupling strength A under the resonance condition. We also assume the initial state $|\Psi(0)\rangle = |-\frac{3}{2}\rangle$. Note that the GHZ state generation time is significantly shortened by applying a stronger laser pulse. This is important because a short pulse length for GHZ state generation is fundamental to observe this high entangled state experimentally.

5. Implementation of Grover's algorithm in three QDs coupled by a single-frequency optical field

Finally we consider the case when the QDs are coupled by an optical field with a single frequency ω. In this case, the Hamiltonian in the rotating frame ($|\Psi(t)\rangle_s = U(t)|\Psi(t)\rangle_U = \mathrm{e}^{-\mathrm{i}\omega J_z t}|\Psi(t)\rangle_U$) becomes [11]

$$H_U = (\varepsilon - \omega)J_z + V(J^2 - J_z^2) + AJ_+ + AJ_- = \Delta_\omega J_z + V(J^2 - J_z^2) + AJ_+ + AJ_-. \tag{25}$$

Here $\Delta_\omega = \varepsilon - \omega$ is the detuning parameter. Following [11], we obtain the effective Hamiltonian:

$$H_U = \begin{pmatrix} \frac{3V}{2} - \Delta_\omega & \sqrt{3}A & 0 & 0 \\ \sqrt{3}A & \frac{7V}{2} - \frac{\Delta_\omega}{2} & 2A & 0 \\ 0 & 2A & \frac{7V}{2} + \frac{\Delta_\omega}{2} & \sqrt{3}A \\ 0 & 0 & \sqrt{3}A & \frac{3V}{2} + \frac{\Delta_\omega}{2} \end{pmatrix}. \tag{26}$$

In resonance $\Delta_\omega = 0$, diagonalization leads us to the following eigenenergies:

$$\begin{aligned} E_{1,2} &= \frac{5V}{2} + A \pm \sqrt{(V + A)^2 + 3A^2}, \\ E_{3,4} &= \frac{5V}{2} - A \pm \sqrt{(V - A)^2 + 3A^2}, \end{aligned} \tag{27}$$

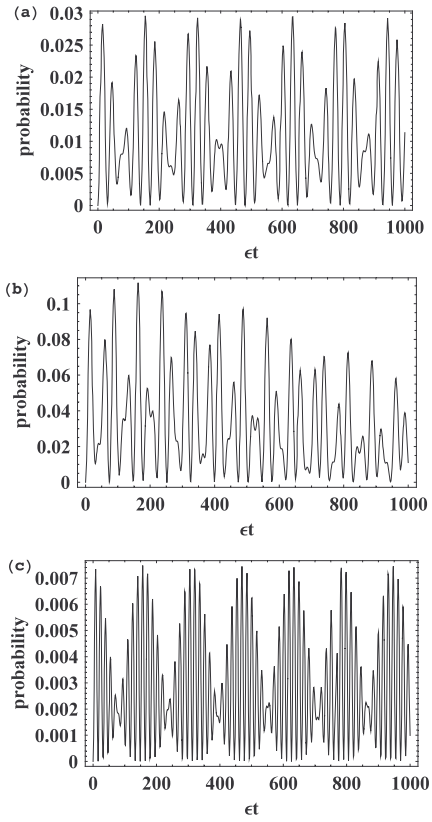

Figure 10. Time-evolution of the one-exciton state $|-\frac{1}{2}\rangle$ in three coupled QDs: (a) $A = 0.01\varepsilon$, $V = 0.1\varepsilon$, (b) $A = 0.02\varepsilon$, $V = 0.1\varepsilon$, (c) $A = 0.01\varepsilon$, $V = 0.2\varepsilon$.

with eigenvectors

$$\begin{aligned}|\varphi_{1,2}\rangle &= \eta_{1,2}\left[\left|-\frac{3}{2}\right\rangle + \frac{E_{1,2}-\frac{3}{2}V}{\sqrt{3}A}\left|-\frac{1}{2}\right\rangle + \frac{E_{1,2}-\frac{3}{2}V}{\sqrt{3}A}\left|\frac{1}{2}\right\rangle + \left|\frac{3}{2}\right\rangle\right],\\ |\varphi_{3,4}\rangle &= \eta_{3,4}\left[\left|-\frac{3}{2}\right\rangle + \frac{E_{3,4}-\frac{3}{2}V}{\sqrt{3}A}\left|-\frac{1}{2}\right\rangle - \frac{E_{3,4}-\frac{3}{2}V}{\sqrt{3}A}\left|\frac{1}{2}\right\rangle - \left|\frac{3}{2}\right\rangle\right],\end{aligned} \tag{28}$$

where the coefficients

$$\eta_i = \frac{1}{\sqrt{2}}\left[1 + \left(\frac{E_i - \frac{3}{2}V}{\sqrt{3}A}\right)^2\right]^{-\frac{1}{2}}, \tag{29}$$

with $i = 1, 2, 3, 4$. The total wave function and the probability of finding the state $|m\rangle$ can also be expressed as equations (16) and (19). We vary the coupling strength A and the interdot Coulomb interaction V to show how the parameters can affect the implementation of Grover's algorithm. Obviously, the probabilities of finding the excited states increase by increasing A or reducing V (see figure 10). The competition of these two terms is usually driven by the competition between kinetic and interaction energy which is fundamental to quantum phase transitions [17]. As an instance to see the advantage of the use of the multiphoton transition schemes proposed by Leuenberger and Loss in [4] and [5] on the implementation of Grover's algorithm, figure 11 shows that when the system is coupled by a single-frequency external field, the probabilities of the excited states are much lower than those of the system coupled

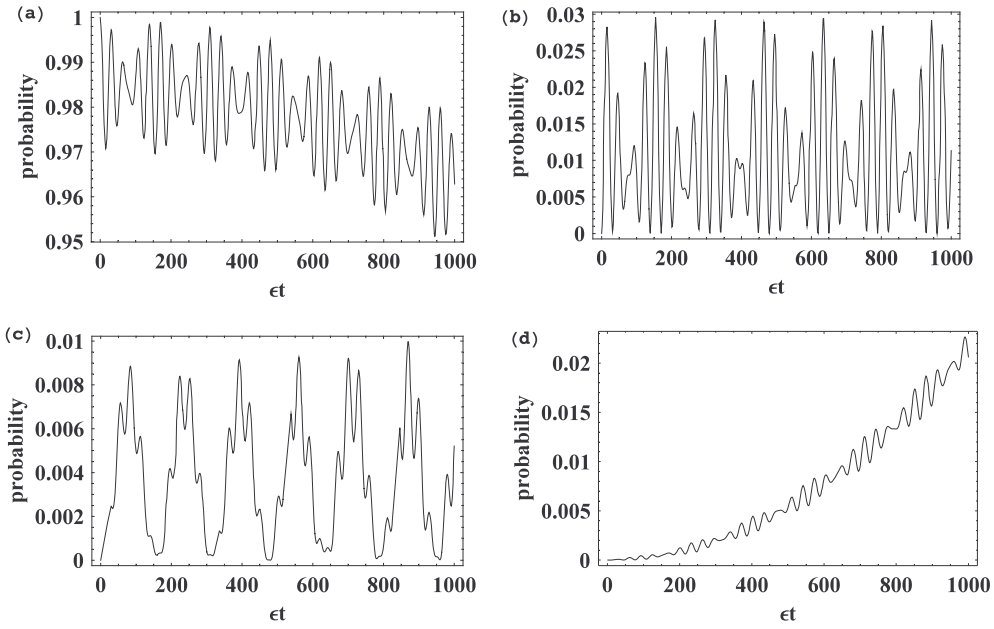

Figure 11. The probabilities of (a) the vacuum state $|-\frac{3}{2}\rangle$, (b) the one-exciton state $|-\frac{1}{2}\rangle$, (c) the biexciton state $|\frac{1}{2}\rangle$, (d) the triexciton state $|\frac{3}{2}\rangle$ in the three QDs coupled by a single-frequency external field. The parameters are $A = 0.01\varepsilon$, $V = 0.1\varepsilon$.

by a multi-frequency field with the same condition. Therefore, the contribution of the triple quantum coherence between $|-\frac{3}{2}\rangle$ and $|\frac{3}{2}\rangle$ can be neglected in the case of weak coupling. Our model also can be used to explain the result reported in [6], in which at low B_1, spectra of ΔR show three oscillations corresponding to the multi-frequency excitation. Only by increasing B_1 to a large value could a new peak corresponding to the single-frequency excitation appear.

6. Conclusions

Due to the potential scalability and long decoherence times of the electron spins [11], the solid-state QD system has been extensively studied for the realization of a quantum computer. Experimental observation of these quantum dots should be possible with present ultrafast semiconductor optical techniques. As an instance, for GaAs QDs $\varepsilon = 1.4$ eV corresponds to a resonant frequency $\omega = 2 \times 10^{-15}$ s^{-1}. Femtosecond spectroscopy could satisfy this system obviously. A monolithic semiconductor device integrated with a point contact channel [6] may be another suitable experimental system for our Hamiltonian. The channel consists of Ga^{69}, Ga^{71} and As^{75}, each having total spin $I = 3/2$. Under the static magnetic field B_0, each nuclide has four equally spaced energy states $|m\rangle = |3/2\rangle, |1/2\rangle, |-1/2\rangle, |-3/2\rangle$. In the meantime, the nuclei experience the effects of an electric field gradient due to their host crystal, which shifts the energy states through the electric quadrupolar interaction by energies $-V$ and V for $|\pm 3/2\rangle$ and $|\pm 1/2\rangle$. The effect results in non-equidistant energy levels, which agrees with our model (see figure 1) for implementing Grover's algorithm.

In summary, we have studied the implementation of Grover's algorithm using the system of three identical QDs coupled by a multi-frequency external field based on the proposal provided by Leuenberger and Loss [4, 5] by means of analytically solving the Schrödinger equation in

the rotating frame. Our result shows that increasing the electric field strength A speeds up the oscillations of the occupations of the excited states rather than increases the occupation probabilities of those states. The larger the detuning of the field from resonance, the fewer the states which can be used as qubits. We also have considered the probability of finding the GHZ state for this system: the GHZ state generation time is significantly shortened by applying a stronger laser pulse. Compared with a multi-frequency external field, a single-frequency external field will generate much lower amplitudes of the excited states under the same coupling strength A and interdot Coulomb interaction V. However, these amplitudes increase on increasing the coupling strength A or decreasing the interdot Coulomb interaction V.

References

[1] Grover L K 1997 *Phys. Rev. Lett.* **79** 325
[2] Grover L K 1997 *Phys. Rev. Lett.* **79** 4709
[3] Ekert A and Jozsa R 1996 *Rev. Mod. Phys.* **68** 733
[4] Leuenberger M N and Loss D 2001 *Nature* **410** 789
[5] Leuenberger M N, Loss D, Poggio M and Awschalom D D 2002 *Phys. Rev. Lett.* **89** 207601
[6] Yusa G, Muraki K, Takashima K, Hashmoto K and Hirayama Y 2005 *Nature* **434** 1001
[7] Leuenberger M N and Loss D 2003 *Phys. Rev.* B **68** 165317
[8] Ahn J, Weinacht T C and Buchsbaum P H 2000 *Science* **287** 463
[9] Bonadeo N H, Chen G, Gammon D, Katzer D S, Park D and Steel D G 1998 *Phys. Rev. Lett.* **81** 2759
[10] Bonadeo N H, Erland J, Gammon D, Katzer D S, Park D and Steel D G 1998 *Science* **282** 1473
[11] Quiroga L and Johnson N F 1999 *Phys. Rev. Lett.* **83** 2270
[12] Biolatti E, Iotti R C, Zanardi P and Rossi F 2000 *Phys. Rev. Lett.* **85** 5647
[13] Biolatti E, D'Amico I, Zanardi P and Rossi F 2002 *Phys. Rev.* B **65** 075306
[14] Lovett B W, Reina J H, Nazir A and Briggs G A 2003 *Phys. Rev.* B **68** 205319
[15] Teich W G, Obermayer K and Mahler G 1988 *Phys. Rev.* B **37** 8111
[16] Greenberger D M, Horne M A, Shimony A and Zeilinger A 1990 *Am. J. Phys.* **58** 1131
[17] Markus G, Olaf M, Tilman E, Theodor W H and Immanuel B 2002 *Nature* **415** 39
Markus G, Olaf M, Tilman E, Theodor W H and Immanuel B 2004 *Nature* B **346/347** 211